Mon. Not. R. Astron. Soc. 000, 1–13 (2003) Printed 27 October 2004 (MN LaTeX style file v2.2)

Revealing the nature of double-periodic blue variables in the Magellanic Clouds

R. E. Mennickent[1*] L. Cidale[2], M. Diaz[3], G. Pietrzyński[1,4], W. Gieren[1], B. Sabogal[1]

[1] Departamento de Fisica, Facultad de Ciencias Fisicas y Matemáticas, Universidad de Concepción, Casilla 160-C, Concepción, Chile
[2] Facultad de Ciencias Astronómicas y Geofísicas, Univ. Nacional de La Plata, Paseo El Bosque S/N, 1900 CCiA, La Plata, Argentina
[3] Instituto de Astronomia, Geofísica e Ciencias Atmosféricas, Universidade de São Paulo, CP 3386, 01060-970 São Paulo, Brazil
[4] Warsaw University Observatory, AL. Ujazdowskie 4, 00-478 Warszawa, Poland

Accepted XXX. Received XXX; in original form XXX

ABSTRACT

We present the first spectroscopic data for a sample of the recently discovered blue double periodic variables in the Magellanic Clouds. The optical spectrum of these objects is dominated by Balmer and Helium absorption lines and a continuum with a blue or sometimes flat slope. Spectral classification yields B spectral types and luminosity classes mostly of type III. However, the Hβ absorption line is weaker than expected for the spectral classification in most objects. For two objects, OGLE05060009-6855025 and OGLE05195898-6917013 we obtained time-resolved spectroscopy, finding radial velocity variations consistent with binarity. Phasing the short-term photometric variability of these two systems with their spectroscopic ephemeris, we find that they can be interpreted as ellipsoidal variations of the brighter component in a close binary system. From the analysis of their short-term light curves and radial velocities, we estimate that the cooler component could be a B-type dwarf. Our findings support the hypothesis that double periodic variables are close binary systems consisting of two B-type stars. The shorter periodicity in non-eclipsing systems should be the ellipsoidal variation of the more evolved component. Regarding the long-term periodicity, we find their origin in or around the brighter star, since the oscillations virtually disappear at primary eclipse. Their origin remains unknown, at the present time. We report also the discovery of three (two of them eclipsing) new double-periodic variables in the *LMC*. One of them shows a shortening of the long-term period by about 20% in a couple of cycles, which coincides with an increase of the maximum oscillation brightness.

Key words:
binaries, stars: early type, stars: evolution, stars: mass-loss

1 INTRODUCTION

A new type of variable stars have been recently discovered in the Magellanic Clouds (Mennickent et al. 2003, hereafter M03) based on an inspection of the OGLE-II photometric database (Zebrun et al. 2001). These authors describe thirty stars showing two kinds of photometric periodic variability: a short-term cyclic variability with typical amplitude $\Delta I \sim 0.05$ mag and period P_1 between 4 and 16 days and a sinusoidal, long-term cyclic oscillation with much larger amplitude $\Delta I \sim 0.2$ mag with period P_2 in the range of 150-1000 days. M03 found that both periods seem to be coupled through the relationship $P_2 = 35.2(8)\ P_1$. In general, the short term variability is reminiscent of those shown by Algol-type binaries, and M03 have proposed that the long-term oscillation could arise in the precession of an elliptical disc fed by a Roche-lobe filling companion in a low mass ratio Algol system.

We have started spectroscopic observations aimed at confirming the binary hypothesis and determine the spectral types of the components of the double-periodic variables. In this paper we present our first results on visual spectroscopy of seven double periodic variables obtained in Chile in the spring of 2003.

* E-mail: rmennick@astro.cfm.udec.cl.

Table 1. The double-periodic variables observed spectroscopically. We give the short (P_1) and the long (P_2) photometric periods with their errors. Sw and dw mean a short-term light curve characterized by a single or a double wave, respectively. The eclipsing systems are labeled with "e".

star	$< V >$	$< B-V >$	$< V-I >$	P_1 (days)	P_2 (days)	Note
OGLE00451755-7323436	17.51	0.306	0.222	5.178(05)	171(15)	dw
OGLE00553643-7313019	17.74	0.079	0.268	5.092(05)	176(17)	dw
OGLE05060009-6855025	15.54	-0.019	0.081	3.849(07)	230(22)	sw
OGLE05155332-6925581	15.58	-0.080	0.039	7.2835(16)	188(11)	e
OGLE05195898-6917013	15.94	-0.022	0.042	2.41(10)	140(05)	sw
OGLE05313130-7012584	15.40	0.016	0.230	9.231(21)	960(176)	sw
OGLE05410942-7002215	17.23	0.269	0.430	6.586(09)	245(23)	dw

2 OBSERVATIONS

Spectroscopic observations were conducted at CTIO, LCO and La Silla Observatory during year 2003. At CTIO we used the 1.5m telescope with the Cassegrain Spectrograph and the Loral 1K detector. Grating # 26 tilted at 15.95 degree, and a slit width of 2 arcsecond yielded a spectral range of 3500-5300 Å, and a resolution of 2 Å. Wavelength calibration functions with typical standard deviation of 0.1 Å were obtained with around 30 He-Ar lines for the comparison spectra. Observations of the standard star LTT 2415 were used for flux calibrations. At La Silla we used the NTT with the EMMI blue branch in medium dispersion grating mode, with grating # 4. This instrumental setup along with a 1 arcsec slit yielded a spectral range of 3500-5050 Å and a resolution of 5 Å. The standard stars EG21 and LTT 377 were observed with 5 arcsec slit, allowing flux calibrations for science spectra. At LCO we used the Irénée du Pont 2.5m telescope with the Modular Spectrograph and the SiTe2 detector. The combination of grating # 600 blazed at 5000 Å, with a slit width of 1.5 arcsec, yielded a spectral range of 4000-6050 Å, and a resolution of 2.5 Å. About 60 He-Ar-Fe lines in the comparison spectra yielded wavelength calibration functions with standard deviation of 0.2-0.3 Å. The targets are listed in Table 1 and details of the observations are given in Table 2.

3 RESULTS

Before giving the spectroscopic results we introduce three newly discovered double periodic variables which are important for the discussion of the phenomenon in Section 4.

3.1 New double-periodic variables found in the OGLE photometric databases

In the course of our search for Be stars in the Magellanic Clouds (Mennickent et al. 2002, hereafter M02) based on the OGLE catalogue (Zebrun et al. 2001), we have discovered other three new double-periodic variables in the *LMC* which were missed by M03. They are OGLE05052263-6852002, OGLE05082755-6937251 and OGLE05200407-6936391. These stars are listed in Table 3 along with their average V magnitude and colours and the result of our period finding analysis. We find short (P_1) and long (P_2) photometric periods with values in the same range as for other double periodic variables. The light curves for these objects are shown in Figs. 1-3, revealing the long-term periodicity and the character of the short-term variability. Two stars are eclipsing binaries, OGLE05052263-6852002 and OGLE05200407-6936391, showing two unequal minima in the short-term light curve. From the depth of the minima we find that the cooler component has an effective temperature roughly 90% the temperature of the hotter component. This is typical for the double periodic eclipsing binaries reported by M03; in fact, analysing their light curve minima we have found temperatures for the cooler component between 81% and 94% of the temperature of the hotter component. Consistently, the same light curves reveal no significant colour modulation during the orbital cycle. In addition, we find that the short and long-term periods of OGLE05052263-6852002 and OGLE05082755-6937251 closely follow the empirical relationship discovered by M03, namely $P_2 = 35.2(8).P_1$. The case of the eclipsing OGLE05200407-6936391 is very interesting, since this star is the only double periodic variable largely deviating from this relationship. The predicted value 353 days, is too long compared with the observed value of 270 ± 20 days. In particular, this star presents a long-term light curve that it is not strictly sinusoidal, but it shows two maxima of different amplitude. Figure 4 shows a zoom into the long-term light curve of this variable and the phase curve obtained folding the data with the 270 day periodicity. The anomaly around phase 1 is evident. The peculiarity of this star is confirmed in the MACHO database; the long-term modulation changed from a period of 340 days (close to the predicted value) which was observed between HJD 2 448 800 and 2 450 000 to a period near to 270 days around HJD 2 450 500, while the maximum brightness of the modulation increased (Fig. 5). This interesting result places securely strong constraints on the possible models aimed to explain the long term variability. For instance, any proposed mechanism should be able to explain: (i) the smooth development of the oscillation amplitude (ii) the time scale involved in the phenomenon (iii) the fact that the period decreases while the amplitude of the oscillation increases and (iv) the abrupt colour change before HJD 2 449 000. The fact that the long-term variability in DPVs could be a not strictly periodic phenomenon was recently pointed out by Mennickent et al. (2004).

The large fraction of eclipsing binaries (6 cases, OGLE05171401-6936374 was probably misclassified as eclipsing binary in M03) found in the whole sample of 33 double periodic variables is amazing. The probability of identifying this kind of variable seems to depend on the system inclination, being larger for high inclination systems.

Table 2. Observing log. We give the number of spectra n, the exposure time in seconds, and the heliocentric julian day for the beginning and the end of the time series (HJD-range). For ESO observations, the HJD zero point is 2 452 800, and for CTIO and LCO observations is 2 452 900.

Run	ut-date	star	n	exptime	HJD-range
ESO	03/09/03	OGLE05410942-7002215	4	300	85.8242-85.8375
ESO	03/09/03	OGLE05313130-7012584	3	600	85.7924-85.8072
ESO	03/09/03	OGLE00451755-7323436	3	600	85.7022-85.7170
ESO	03/09/03	OGLE00553643-7313019	3	600	85.7332-85.7479
ESO	03/09/03	OGLE05060009-6856025	3	600	85.7646-85.7793
CTIO	30/10/03	OGLE05060009-6856025	26	600	42.6160-42.8652
CTIO	30/10/03	OGLE05155332-6925581	6	600	42.7616-42.8485
CTIO	31/10/03	OGLE05060009-6856025	27	600	43.6367-43.8424
CTIO	01/11/03	OGLE05060009-6856025	18	600	44.6366-44.8211
CTIO	02/11/03	OGLE05060009-6856025	26	300	45.6633-45.8637
CTIO	02/11/03	OGLE05195898-6917013	23	300	45.6365-45.8378
CTIO	03/11/03	OGLE05060009-6856025	32	300	46.6248-46.8484
CTIO	03/11/03	OGLE05195898-6917013	24	300	46.6500-46.7904
LCO	12/11/03	OGLE05060009-6856025	8	300	55.6165-55.8362
LCO	13/11/03	OGLE05060009-6856025	8	300	56.6317-56.8575
LCO	14/11/03	OGLE05060009-6856025	5	300	57.6094-57.6247
LCO	15/11/03	OGLE05060009-6856025	6	300	58.7091-58.7282
LCO	12/11/03	OGLE05195898-6917013	10	300	55.6345-55.8599
LCO	13/11/03	OGLE05195898-6917013	6	300	56.6509-56.6700
LCO	14/11/03	OGLE05195898-6917013	6	300	57.6320-57.6510
LCO	15/11/03	OGLE05195898-6917013	5	300	58.7345-58.7498

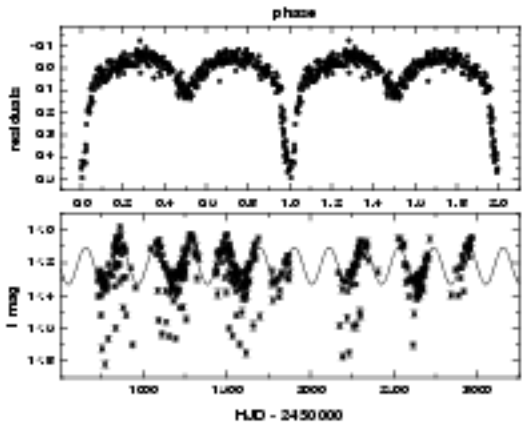

Figure 1. Long-term light curve of OGLE05052253-6852002 and the best sinus fit (bottom) and residuals folded with the short-term period (up).

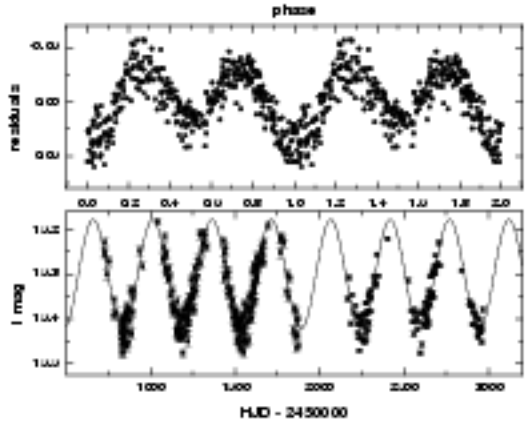

Figure 2. Long-term light curve of OGLE05082755-6937251 along with the best sinus fit (bottom) and residuals folded with the short-term period (up).

We suspect that many of the Type-3 stars reported by M02 and not classified as double periodic variables are the same kind of system but seen at lower inclination. In these cases the amplitude of the short-term oscillation could be undetected only by a projection factor. This is consistent with an interpretation as ellipsoidal variations of a gravitationally distorted star in a close binary system. This view is also supported by the observations discussed in Section 3.4.

3.2 Spectroscopy of 7 double periodic variables

The average spectra of the seven double periodic variables observed spectroscopically are shown in Fig.6. We averaged 47 CTIO spectra for OGLE05195898-6917013, 6 CTIO spectra for OGLE05155332-6925581, 4 NTT spectra for OGLE05410942-7002215 and 3 NTT spectra for each of the others. The relative strength of CaII 3933 and He, along with the presence of He4471, suggests a B-type spectral classification for most objects. Particularly interesting is the flattening of some spectra, like those of OGLE05410942-7002215, OGLE00451755-7323436 and OGLE00553643-7313019 and the weakness of the $H\beta$

Table 3. The new double-periodic variables in the *LMC*. We give the short (P_1) and the long (P_2) photometric periods with their errors. Dw means double wave and e eclipsing. HJD_0 is the time for the main minimum of the short-term light curve (+2 450 000).

star	$<V>$	$<B-V>$	$<V-I>$	P_1 (days)	P_2 (days)	HJD_0	Note
OGLE05052263-6852002	17.471	0.063	0.218	6.2968(30)	207 (15)	732.0152 (38)	e
OGLE05082766-6937251	15.528	0.088	0.172	9.7676(20)	351 (45)	731.0276(260)	dw
OGLE05200407-6936391	14.976	-0.099	-0.031	10.0316(03)	270 (20)	453.0145 (59)	e

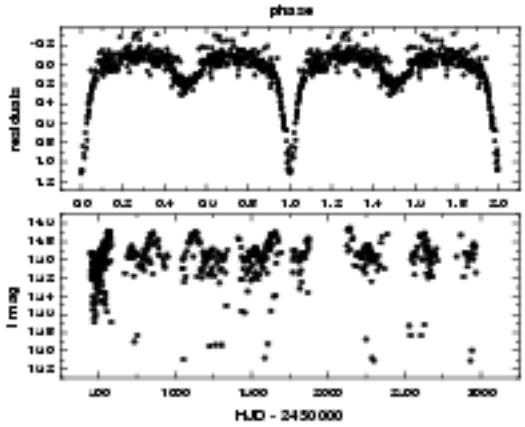

Figure 3. Long-term light curve of OGLE05200407-6936391 (bottom). This light curve was folded with the long-term period and a fourth order polynomial was fitted. Residuals to this polynomial are shown phased with the short-term period in the upper graph. The choice of a different pre-whitening function have not a significant effect on our conclusions (see Section 4.2).

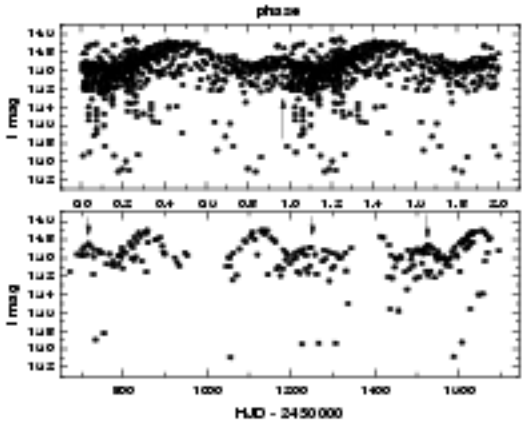

Figure 4. The bottom graph shows a zoom into the long-term light curve of OGLE05200407-6936391. Secondary maxima are indicated with arrows. The upper graph shows the light curve folded with the long-term period of 270 days. Phase zero is HJD 2450453.0145. The region where the secondary maxima appear is indicated by an arrow.

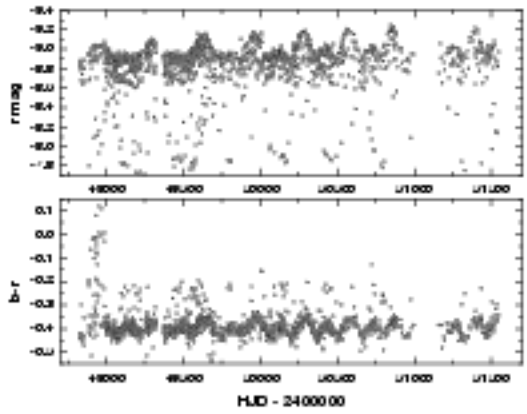

Figure 5. The long-term MACHO light curve of OGLE05200407-6936391 showing the development of the long-term variability and the shortening of the period.

absorption line, especially in OGLE00451755-7323436 and OGLE00553643-7313019, the only two stars in the *SMC* in our sample.

The spectral classification of the stars observed spectroscopically was derived considering both the *BCD* (Barbier-Chalonge-Divan) spectrophotometric system and the measurement of the equivalent width of some selected lines (Didelon 1982). The *BCD* stellar classification system, was introduced by Barbier & Chalonge (1941) and Chalonge & Divan (1952). It is based on measurable quantities of the Balmer discontinuity (BD). This system is useful for stars ranging from spectral type O4 to F9 where the BD is larger than about 0.005 dex. In the λ 3500-4600Å region two spectrophotometric parameters are defined: D in dex and λ_1, this last is commonly presented as the difference λ_1-3700 Å. D is a measure of the Balmer jump at λ 3700 Å, which is obtained by extrapolating the Paschen continuum energy distribution in a $\log F_\lambda/B_\lambda$ vs. $1/\lambda$ display (B_λ is a reference flux distribution of known temperature). λ_1 gives the mean spectral position of the BD. D is a strong indicator of the effective photospheric temperature and λ_1 is related to the photospheric log g parameter. The *BCD* parameters have the advantage that they are not affected either by interstellar extinction or by circumstellar absorption and/or emission. Therefore, the *BCD* system is also suitable for the spectral classification of objects with circumstellar material, even for those peculiar stars showing the B[e] phenomenon (Cidale, Zorec, & Tringaniello 2001). From the observed (λ_1, D) BCD parameters we can determine the fundamental parameters

of stars (T_{eff}, $\log g$, M_V, M_{bol}) and the spectral type using the calibrations of (λ_1, D) given by Divan & Zorec (1982) and Zorec (1998). The advantages and uncertainties of determining fundamental parameters are discussed in Divan & Zorec (1982) and Zorec & Briot (1991).

The results of the *BCD* spectral classification are shown in Table 4. We confirm the B-type classification for all objects. Most stars are classified as giants, coinciding with their position above the main sequence (see Section 4). Only the two objects in the SMC, OGLE00451755-7323436 and OGLE00553643-7313019, are spectroscopically classified as dwarfs. However these objects, along with OGLE05410942-7002215, turned to be very hard to classify since their spectra display either a small Balmer discontinuity or a small S/N ratio. These objects show a very peculiar flat continuum with weak absorption lines, and their *BCD* classification turned to be more uncertain.

When interpreting the flux distribution and colour of double periodic variables, we should consider how binarity (which is probed in Section 3.4) affects the *BCD* classification. We investigated the MACHO short-term light curves for the three objects showing peculiar flux distributions and find no colour variation during the orbital cycle. This is consistent with our results of Section 4 indicating dwarf-like secondaries. Hence, the peculiar flux distribution in these objects cannot be attributed to merging of stellar continuum at different temperatures. Assuming that the Balmer jump represents the contribution of a single star, we estimate errors of ΔD between 0.01 and 0.02. The largest discrepancies correspond to spectra with low S/N ratio. The uncertainties in ΔD yields errors between 500 K and 1500 K for T_{eff}, $\sim$ 0.5 for $\log g$ and ~ 0.5 for M_V.

The spectral type of our sample stars can also be determined by measuring the line equivalent widths. Didelon (1982) showed that the equivalent width of lines like Hβ, He I 4471.48, Mg II 4481.23, He I 4026.19, Si II 3856.02 and He I 4143.76 are indicators of spectral type and luminosity class for the B-type stars. However, the solutions in many cases are not unique, and different classifications are sometimes possible for the same set of parameters. In general, stars with spectral types either in the range B0-B2 or B4-B7 have similar HeI equivalent widths (EW). This fact, along with the issue that many weak lines were measured at the limit of our instrumental resolution, yielded to consider this method as a reference, providing only a range for the possible spectral type classification. Table 5 lists our measurements of EW. These values are consistent with the spectral types derived from the *BCD* spectral classification.

A comparison between spectral types derived from the *BCD* classification and the line spectral analysis (Didelon 1982) shows in general discrepancies from 1 to 2 B subspectral types. In some cases the earliest spectral types correspond to the BCD system which is consistent with the fact that (λ_1, D) parameters are obtained from the continuum energy distribution originating in atmospheric layers deeper than those giving rise to spectral lines.

Table 5 indicates the Hβ line is weaker than expected for the adopted spectral type in most systems (including two of the three peculiar objects). We find the same behaviour for the Hγ absorption line. We discuss the apparent filling by emission in these lines and the colour excess (see below) in Section 4.4.

A comparison of $(B-V)_0$ values computed from OGLE II photometry (assuming uniform reddening for each LMC and SMC OGLE fields, Udalski et. al. 1998, 1999) with $(B-V)_0$ values obtained from spectral data (using color-temperature calibrations, Flower 1977) shows intrinsic reddening for some of the objects listed in Table 4. Such reddening could be presumably due to circumstellar emission and/or to gravity darkening of the underlying star (Slettebak 1985). The major discrepancy $\Delta(B-V)_0$, between 0.25 and 0.45, corresponds to the objects with a peculiar flat continuum and a weak Hβ line absorption, OGLE05410942-7002215, OGLE00451755-7323436 and OGLE00553643-7313019. OGLE05313130-7012584 shows an intrinsic color excess $\Delta(B-V)_0 = 0.17$ which is similar to those found for Be stars in galactic clusters (Slettebak 1985) while the rest of the objects have $\Delta(B-V)_0 < 0.08$.

3.3 Search for variability of the Hβ absorption line in OGLE05060009-6855025 and OGLE05195898-6917013

Equivalent widths were measured by fitting the absorption lines with a gauss function and determining the area under the fit. These measurements were compared with those obtained by directly evaluating the integral flux under the (interpolated) linear continuum along the line full width at zero intensity. The results were consistent, but they showed a mean shift of the values obtained with the later method by +0.4 Å. For OGLE05060009-6855025, we investigated if there was some evidence for variability in the strength of the Hβ absorption line. The mean equivalent width for this line and its standard deviation was 4.3 ± 0.3, 4.4 ± 0.5 and 4.5 ± 0.3 Å for the ESO, CTIO and LCO runs respectively, revealing that the line was stable at the level of 10% during a 2-month interval. In any case, the line is much weaker than expected for a B5III star, by ≈ 2.6 Å. For OGLE05195898-6917013, the corresponding figures were 4.3 ± 0.7 and 3.7 ± 0.4 Å for the CTIO and LCO runs, respectively, indicating a constancy of the line strength at the 15% level and also a filling by emission by an amount similar to OGLE05060009-6855025.

3.4 Radial velocity analysis

We selected two objects, OGLE05060009-6855025 and OGLE05195898-6917013, for a time-resolved radial velocity study. For the time-series obtained at CTIO and LCO, we normalized the spectra fitting the continuum with a low order polynomial. Then we measured radial velocities by cross correlating every spectrum with a reference spectrum, obtained by averaging the best quality spectra per run. For that the IRAF task *fxc* was used. At our resolution, the merging of spectra with different radial velocities is not a problem. The velocities of every spectrum were shifted to an absolute scale correcting by the velocities of every template. The template velocities were obtained by fitting the Balmer lines with gauss functions and finding the central velocity. Very noisy spectra were discarded for further RV analysis, letting 145 spectra for OGLE05060009-6855025 and 102 spectra for OGLE05195898-6917013. Finally, the heliocentric correction was applied to each radial velocity. Results are given in Tables 6 and 7.

Table 4. Results of the *BCD* classification. We give the *BCD* parameters D and λ_1 along with the corresponding effective temperature, surface gravity and absolute magnitude, bolometric magnitude and spectral type. The column "Notes" indicates if the equivalent widths of non HI lines are consistent with the *BCD* classification. Cases with weak Hβ absorption are indicated.

star	D	λ_1	T_{eff}	log g	M_{bol}	M_V	Sp	Notes
OGLE00451755-7323436	0.118	52.83	23500	3.8	-5.5	-3.2	B1IV	doubtful, Hβ weak
OGLE00553643-7313019	0.115	81.41	26500	4.2	-5.5	-2.0	B1V	yes, Hβ weak
OGLE05060009-6855025	0.240	32.50	13500	2.8	-4.2	-3.2	B5III	doubtful, Hβ weak
OGLE05155332-6925581	0.232	37.63	14700	3.1	-3.7	-2.6	B5III	yes, Hβ weak
OGLE05195898-6917013	0.225	44.36	16000	3.5	-3.7	-2.2	B4III	yes
OGLE05313130-7012584	0.187	43.08	18000	3.3	-4.3	-2.7	B3III	doubtful, Hβ weak
OGLE05410942-7002215	0.095	36.12	20500	2.7	-7.2	-5.5	B0-B1 IV-III	doubtful

Table 5. Equivalent Widths in Å. The error is < 8 % except for Hβ < 15 %. In some cases the measurement was not possible due to line blending, line not visible or noisy spectrum.

star	H$_\beta$	HeI 3819	HeI 4026	HeI 4144	HeI 4388	HeI 4471	MgII 4481
OGLE00451755-7323436		0.94	1.52		1.82	1.67	
OGLE00553643-7313019		1.26		0.62	0.50	1.18	0.83
OGLE05060009-6855025	4.54		0.65	0.27		0.52	
OGLE05155332-6925581	5.65		0.81	0.33	0.35	0.63	0.18
OGLE05195898-6917013	6.47		0.95		0.78	0.59	0.29
OGLE05313130-7012584	3.97	0.66	0.70	0.38		0.68	0.30
OGLE05410942-7002215	6.86		1.53	0.29		0.35	0.64

Our observations were too sparse to search for periodicities in our RV time series. However, we investigated if the velocities were consistent with the idea that the short photometric periods reflected the orbital motion in a binary star. The result of folding the RV data set for OGLE05060009-6855025 with its short photometric period is shown in Fig. 7. The fit is excellent when we use as folding period twice the short photometric period. This empirical result supports, for this object, the assumption made by M03 that P_1 reflects the orbital period in a binary star, and that the single wave character of the light curve in some systems indicates that the true orbital period is twice P_1. The best sinus fit yields an ephemeris $HJD_0 = 2\,452\,899.3083 \pm 0.0837$ for the time of passing through the mean from higher to lower RV. The radial velocity half amplitude is $K = 115 \pm 6$ km s^{-1} and the mean velocity is $\gamma = 290 \pm 4$ km s^{-1}. We did the same exercise for OGLE05195898-6917013, whose short-term light curve also shows a single wave. The result of folding the RV data with twice P_1 is shown in Fig. 8. In this case the best sinus fit yields an ephemeris $HJD_0 = 2\,452\,902.4840 \pm 0.1730$, a radial velocity half amplitude $K = 102 \pm 27$ km s^{-1} and a mean velocity $\gamma = 355 \pm 18$ km s^{-1}. The high γ values found in both systems are consistent with their positions in the Magellanic Clouds (Welch et al. 1991).

We analyzed how the short-term photometric variability ephemeris is related to the spectroscopic ephemeris for OGLE05060009-6855025 and OGLE05195898-6917013. To this end, we fit the long-term light curves obtained from the OGLE databases with sinus functions. The residuals were phased with the spectroscopic ephemeris and the results are shown in Figs. 9 and 10. We find that the short-term photometric variability attains maxima and minima approximately at phases 0.25 and 0.75. The discrepancy of 0.05 cycles for OGLE05195898-6917013 could be due to their lower precision ephemeris. The above finding is important since it reveals that the source of the ellipsoidal variations is the brighter component, the B-type star whose Hβ radial velocity was measured. The rotation of the distorted B-giant produces the short-term photometric variability, the two maxima will be equal since the system is seen broad-side on at maximum and minimum RV. However, the two minima can vary in depth, since the cusp of the first Lagrangian point could be the coolest part of the lobe (by the von-Zeipel law) and give rise to the deeper minimum. Different minima are really observed in the majority of the double-periodic variables, but the two cases under study, OGLE05060009-6855025 and OGLE05195898-6917013, show minima of roughly equal depth. This could indicate a lower inclination for these systems or an underfilling of the Roche lobe.

4 DISCUSSION

4.1 Double-periodic variables as semi-detached binaries

The working hypothesis outlined by M03 suggests that these newly discovered variables are semi-detached binaries experiencing a process of mass transfer. This scenario includes the existence of a gaseous disc precessing in the comoving system of rest. As we will show, this view places severe constraints on the nature of the binary components. The mean density ρ (g cm^{-3}) for a lobe-filling donor star is related to the orbital period P (days) by:

$$P\rho^{1/2} = 0.1375 \left(\frac{q}{1+q}\right)^{1/2} r_L^{-3/2} \quad (1)$$

Table 6. Heliocentric radial velocities (in km s^{-1}) of the Hβ absorption line for OGLE05060009-6855025.

HJD	RV	HJD	RV	HJD	RV	HJD	RV	HJD	RV
2944.6866	290	2942.7950	359	2943.8108	395	2945.8600	198	2946.8365	25
2944.6937	326	2942.8021	365	2943.8179	413	2945.8637	240	2946.8402	154
2944.7008	381	2942.8113	370	2943.8282	422	2946.6248	37	2956.6165	115
2944.7098	408	2942.8184	378	2943.8353	393	2946.6284	272	2956.6203	169
2944.7169	321	2942.8255	358	2943.8424	364	2946.6321	224	2956.6241	170
2944.7240	350	2942.8578	371	2945.6633	227	2946.6357	235	2956.8248	148
2944.7374	350	2942.8652	383	2945.6669	194	2946.6393	245	2956.8248	143
2944.7446	249	2943.6367	325	2945.6705	297	2946.6430	200	2956.8286	190
2944.7517	409	2943.6439	375	2945.6742	275	2946.6996	263	2956.8324	180
2944.7608	347	2943.6510	383	2945.6778	285	2946.7032	189	2956.8362	176
2944.7679	398	2943.6604	371	2945.6814	200	2946.7069	224	2956.6317	276
2942.6160	421	2943.6675	397	2945.6868	288	2946.7105	216	2956.6355	244
2942.6231	404	2943.6747	358	2945.6904	321	2946.7141	258	2956.6393	275
2942.6302	361	2943.6845	348	2945.6940	257	2946.7178	233	2956.6431	273
2942.6391	413	2943.6916	391	2945.6977	328	2946.7232	161	2956.8461	242
2942.6462	389	2943.6987	399	2945.7013	325	2946.7268	157	2956.8499	293
2942.6533	419	2943.7076	414	2945.7049	276	2946.7304	133	2956.8537	313
2942.6627	415	2943.7147	388	2945.7671	376	2946.7341	231	2956.8575	276
2942.6698	441	2943.7218	407	2945.7708	443	2946.7413	246	2957.6094	346
2942.6769	436	2943.7308	445	2945.7744	406	2946.7985	213	2957.6132	384
2942.6928	394	2943.7379	446	2945.7780	283	2946.8022	235	2957.6171	348
2942.6999	430	2943.7451	406	2945.7817	258	2946.8058	187	2957.6209	332
2942.7087	399	2943.7539	393	2945.7853	438	2946.8094	239	2957.6247	341
2942.7158	373	2943.7610	341	2945.7934	206	2946.8131	170	2958.7092	338
2942.7229	422	2943.7681	422	2945.7970	194	2946.8167	200	2958.7130	429
2942.7321	416	2943.7771	392	2945.8006	284	2946.8220	216	2958.7168	418
2942.7392	402	2943.7842	433	2945.8043	265	2946.8256	168	2958.7206	351
2942.7464	433	2943.7913	401	2945.8079	232	2946.8293	253	2958.7244	419
2942.7879	359	2943.8037	413	2945.8115	337	2946.8329	128	2958.7282	352

Table 7. Heliocentric radial velocities (in km s^{-1}) of the Hβ absorption line for OGLE05195808-6917013.

HJD	RV	HJD	RV	HJD	RV	HJD	RV	HJD	RV
2945.6391	394	2945.8378	230	2946.7795	341	2957.6358	326	2956.6509	171
2945.6428	619	2946.6500	375	2946.7832	373	2957.6396	338	2956.6548	202
2945.6464	355	2946.6536	290	2946.7868	221	2957.6434	312	2956.6586	290
2945.6500	496	2946.6572	289	2946.7904	307	2957.6472	256	2956.5803	210
2945.6537	657	2946.6609	256	2956.6345	139	2957.651	296	2956.6662	270
2945.7137	461	2946.6645	400	2956.6383	347	2958.7345	393	2956.6700	255
2945.7174	399	2946.6681	357	2956.6421	348	2958.7383	517	2957.6320	374
2945.7210	439	2946.6735	488	2956.6459	292	2958.7422	404	2957.6358	242
2945.7246	402	2946.6772	101	2956.6497	235	2958.746	566	2957.6396	330
2945.7319	485	2946.6808	303	2956.8447	229	2958.7498	291	2957.6434	320
2945.7372	405	2946.6844	361	2956.8485	109	2958.7345	385	2957.6472	315
2945.7409	383	2946.6881	224	2956.8523	272	2956.6345	293	2957.6510	349
2945.7445	371	2946.6917	469	2956.8561	276	2956.6383	352	2958.7345	486
2945.7481	438	2946.7488	135	2956.6791	321	2956.6421	384	2958.7383	422
2945.7518	486	2946.7524	219	2956.6509	269	2956.6459	210	2958.7422	421
2945.7554	384	2946.7560	359	2956.6548	247	2956.6497	191	2958.7460	476
2945.8197	716	2946.7597	413	2956.6586	285	2956.8447	168	2958.7498	396
2945.8233	480	2946.7633	455	2956.5803	282	2956.8485	169	2958.7345	485
2945.8269	401	2946.7669	358	2956.6662	243	2956.8523	297		
2945.8306	401	2946.7723	260	2956.6700	326	2956.8561	274		
2945.8342	561	2946.7759	401	2957.6320	269	2956.6791	399		

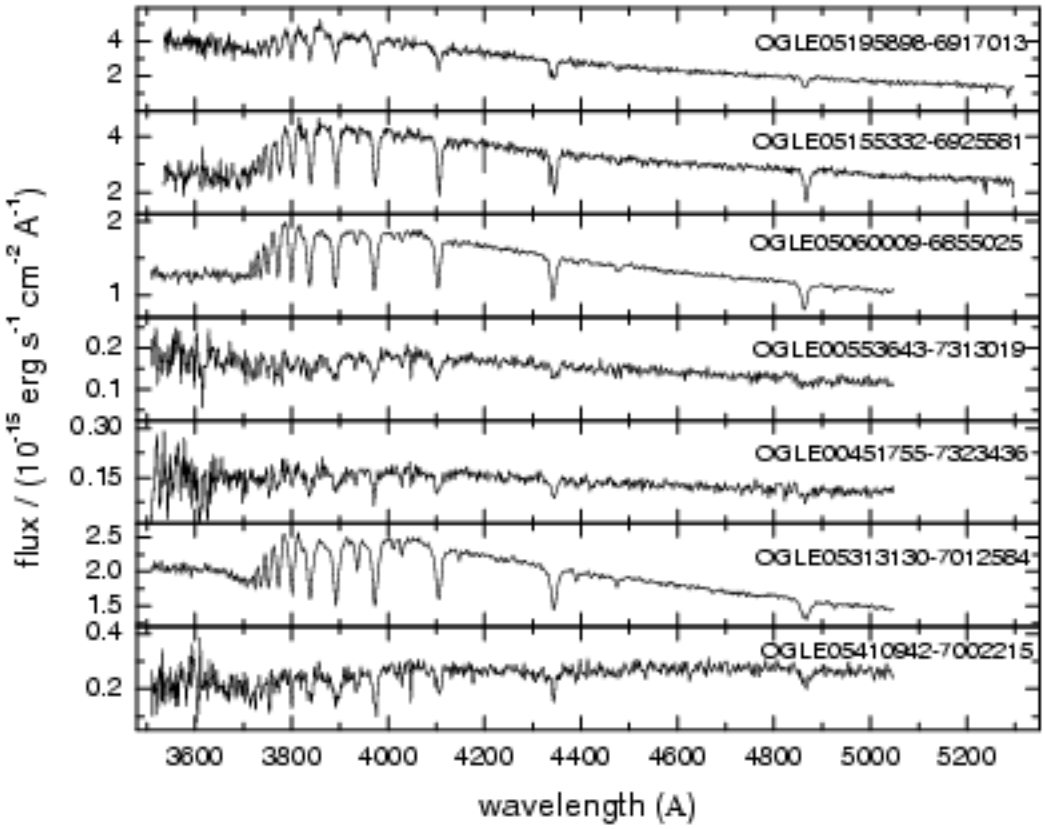

Figure 6. Average spectra for double-periodic blue variables.

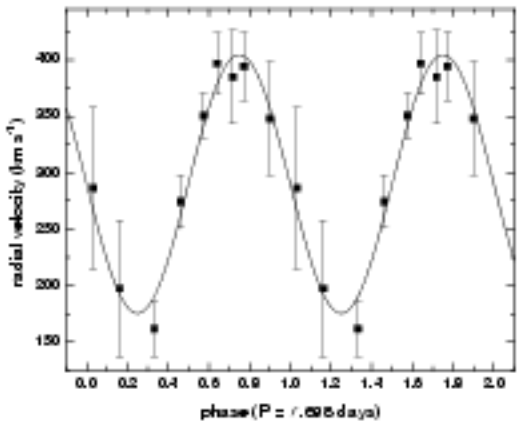

Figure 7. OGLE05060009-6855025 radial velocities folded with twice the short photometric period. For best visualization, we show the average of the RV's per phase bin, along with its standard deviation as error bars.

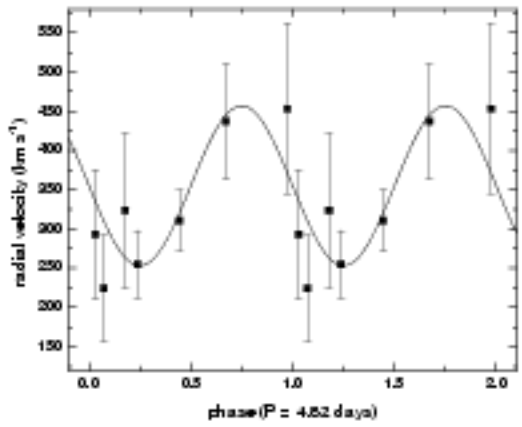

Figure 8. Same as Fig. 7 for OGLE05195898-6917013.

(Eggleton 1983), where r_L is in units of the orbital separation and can be approximated, to better than 1% over the

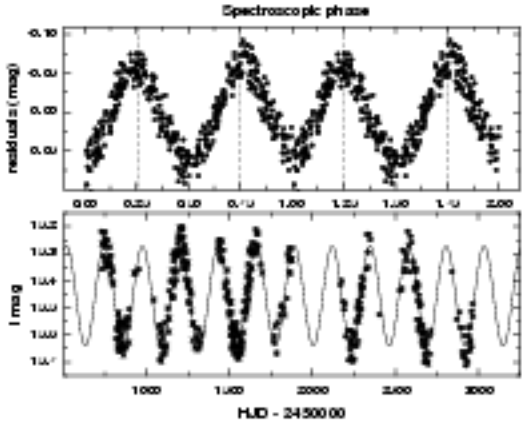

Figure 9. The bottom panel shows the long-term OGLE light curve for OGLE05060009-6855025 and the best sinus fit. The upper panel shows the residuals of this fit folded with the spectroscopic ephemeris.

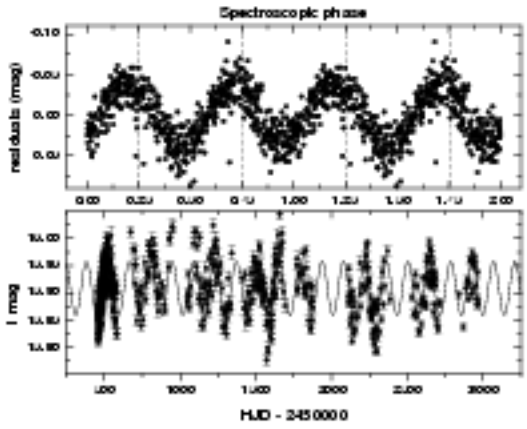

Figure 10. Same as Fig. 9 for OGLE05196898-6917013.

whole range of mass ratios q (M_2/M_1) as:

$$r_L = \frac{0.49q^{2/3}}{0.6q^{2/3} + \ln(1+q^{1/3})} \qquad (2)$$

(Eggleton 1983). Hence, $P\rho^{1/2}$ is a function of q only and over the range $0.01 \leqslant q \leqslant 10$, varies by less than 20% from the value 0.37. In the following, the index 2 refers to the donor star (the brighter, primary star) and 1 to the mass-gaining companion (the fainter, secondary star).

For periods between 5 and 18 days, as are observed in double-periodic variables, we found average densities between 5×10^{-3} and 4×10^{-4} g cm^{-3}, corresponding to O-K giants or O-B supergiants (Cox 2000).

In addition, to allow disc formation, the so called circularization radius R_{circ} should be larger than the radius of the mass-gaining star. The circularization radius for Roche lobe overflow is given by:

$$R_{circ} \cong 4(1+q)^{4/3}\left[0.500 - 0.227\log q\right]^4 P^{2/3} R_\odot \qquad (3)$$

(Frank, King, & Raine 2002). For an orbital period of 5 days this formula yields a circularization radius between 5 and 1.6 $R_\odot$ for $0.05 \leqslant q \leqslant 10$. The corresponding figures for a binary with orbital period of 18 days are 11.5 and 3.7 $R_\odot$ respectively. Therefore we conclude that if the hypothesis of disc formation is correct, the mass-gaining star could be a dwarf or even a white dwarf with an accretion disc, although an evolved star of spectral type roughly between B5 and G5 would also fit inside its Roche lobe and even allow some space for disc formation. We discard the massive X-ray binary hypothesis on the basis of lacking X-ray emission. A crosscheck of the targets in the NASA HEASARC (http://heasarc.gsfc.nasa.gov/) reveal only a couple of low probability associations with ROSAT, XMM or CHANDRA sources.

The observation of the colour-magnitude (CM) diagram for the *LMC* double periodic variables reported by M03 along with the three new objects reported earlier in this paper (Fig. 11) shows that these systems have colours and magnitudes consistent with an evolved, rather giant but not supergiant, B-A type star. The three *SMC* double periodic blue stars reported by M03 occupy basically the same position regarding the *SMC* main sequence. Interestingly, this is consistent with the expectation for the donor obtained through Eq. 1 and with the *BCD* classification given in Section 3.2 for most objects studied spectroscopically in this paper.

We conclude that spectroscopy supports, in principle, the scenario of semi-detached binaries for double periodic variables with the donor star as the primary, brighter component.

4.2 On the nature of the cooler component and system parameters

In the case that the short-term variability observed in the light curves of double-periodic variables are the ellipsoidal variations of the brighter component, we could combine the dynamical information obtained from the radial velocity analysis of OGLE05060009-6855025 and OGLE05195898-6917013 with the photometric amplitudes of its short-term variations in order to get constraints on the system inclination and mass ratio.

An expression for the full amplitude of the ellipsoidal variations is given by:

$$\Delta m \ (\mathrm{mag}) \approx \frac{3}{2q} f^3 (R/a)^3 \sin^2 i \ (1+\tau_0)\frac{15+u}{15-5u} \qquad (4)$$

(Russell 1945, McClintock et al. 1983), where f is the radial fraction of the Roche lobe which is filled, i the systemic inclination angle, and R/a the ratio of the Roche lobe radius of the donor star to the distance between the stars. τ_0 and u are the gravity-darkening and limb-darkening coefficient, respectively.

On the other hand, the mass function can be written as:

$$\frac{PK_2^3}{2\pi G} = \frac{M_2 \sin^3 i}{q(1+q)^2} \qquad (5)$$

where K_2 and M_2 are the radial velocity half amplitude

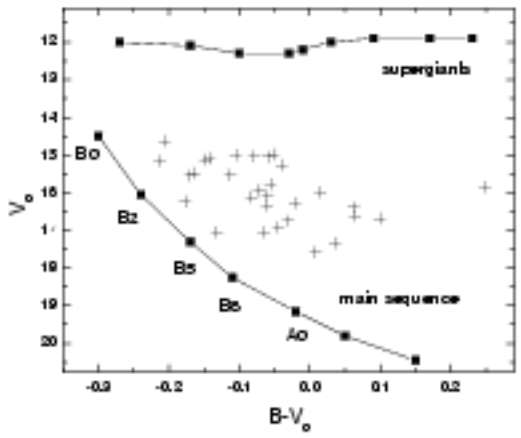

Figure 11. The de-reddened colour-magnitude diagram for the double-periodic stars in the *LMC* reported by M03. Three new stars documented in Section 3.1 are also plotted. We show the main sequence and supergiant location based on Cox (2000) data and using a *LMC* distance module of 18.5. Errors of the OGLE photometry are typically less than 0.02 mag. From this diagram we conclude that most systems are likely evolved. Reddening values for each star were taken from Udalski et al. (1999).

and mass of the donor star, respectively. We can combine both equations in order to get an expression for the mass ratio eliminating $\sin i$. Using $R/a \approx 0.38 + 0.20 \log q$ which is accurate to 2% in the range $0.3 < q < 20$ (Paczynski 1971) we get:

$$\frac{(1+q)^2(0.38+0.20\log q)^{2/2}}{\sqrt{q}} = \frac{\triangle m^{3/2} M_2 C}{P(K_2/213)^3} \qquad (6)$$

where M_2 is in solar masses, P in days, K in km s^{-1} and C is a constant given by:

$$C = \left(\frac{2}{3f^3}\frac{(15-5u)}{(1+\tau_0)(15+u)}\right)^{3/2} \qquad (7)$$

For OGLE05060009-6855025 and OGLE05195898-6917013 limb-darkening coefficients of 0.22 and 0.21 were obtained from Al-Naimiy (1978), who provide a grid of limb-darkening coefficients, calculated from model atmospheres, as a function of effective temperature, wavelength and gravities. For the gravity-darkening coefficient we used the value of 1, for a star whose sub-surface layers transfer energy uniquely by radiation (von Zeipel 1924), but this parameter could be larger even by 50% in highly distorted hot stars filling their Roche lobes in semi-detached binaries (Djuraševič et al. 2003). The factor f was assumed 1. The full amplitude of the ellipsoidal variations were calculated by fitting a sinus function to the long-term residuals phased with the short period. These amplitudes resulted 0.120(1) and 0.072(2) for the I-band light curves of OGLE05060009-6855025 and OGLE05195898-6917013, respectively. We also measured these amplitudes for the $b-r$ MACHO light curves (freely available at http://wwwmacho.mcmaster.ca/), obtaining 0.122(1) and 0.128(2) for the b and r OGLE05060009-6855025 light curves and 0.078(1) and 0.080(1) for the b and r OGLE05195898-6917013 light curves. The fact that the amplitude of the short-term variability in these stars is practically independent of wavelength suggests that the secondary star have a neglectable contribution to the system light in a wide wavelength range. We therefore assume that these amplitudes correspond to the full light amplitude of the primary and we have used these values as $\triangle m$ in Eq. 6.

Using Eq. 6 and assuming $M_2 = 7$ M$\odot$, representative for a B5 III star, we find $q = 0.85 \pm 0.11$ for OGLE05060009-6855025 and q between 0.55 and 1.60 for OGLE05195898-6917013 with the most likely value at 0.9. The errors above consider only the uncertainty in the more sensitive parameter K. Underestimating τ_0 by 50% decreases q down to 0.7 in OGLE05060009-6855025 and up to 0.7 in OGLE05195898-6917013, whereas an uncertainty of 20% in M_2 yields to an error of 13% in q. On the other hand, the underfilling of the Roche lobe by 10% ($f = 0.9$) increases the mass ratio by 38%. The most likely inclination compatible with the quantities derived above is 53° for OGLE05060009-6855025 and 38° degree for OGLE05195898-6917013. Our estimates above suggest that the second component should have a mass between 6-10 M$\odot$ for OGLE05060009-6855025 and OGLE05195898-6917013. This should correspond to an early B-type star. If the radial velocities are not heavily contaminated by an emission source, and reflect the orbital motion of the brighter component, then the possibility of a white dwarf secondary is excluded by the dynamical solution in both systems. In addition, the almost zero contribution to the radiative flux of the secondary star in both systems should indicate a dwarf rather a giant. The circularization radius given by Eq. 3 is 2.5 $R\odot$ for OGLE05060009-6855025 and 1.9 $R\odot$ for OGLE05195898-6917013. This means that disc formation by accretion of material from the primary star is not possible for secondaries fitting the dynamical solution (typical radius for early B-type dwarfs are 7-4 $R\odot$). Another cause besides emission from an accretion disc around the secondary should be invoked to explain the filling by emission of the Balmer absorption lines in these systems.

Our finding above contradicts the hypothesis outlined by M03 that the long-term photometric variability could be due to precession of an elliptical accretion disc in a low mass ratio semi-detached binary. If disc precession is excluded as an explanation, there must be another cause for the long-term variability.

4.3 On the nature of the long-term variability and the pulsation hypothesis

Fig. 12 shows the light curves of OGLE05052263-6852002 and OGLE05200407-6936391 folded with their short-term periods. The remarkable fact in these figures is the vanishing of the long-term variability during the main eclipse. A similar behaviour is observed in all the eclipsing binaries reported by M03; the long-term oscillation always disappear at main minimum but it is present, sometimes with lower amplitude, in the secondary minimum. This can only be interpreted if the main origin of the long-term variations is the brighter star.

We have explored the possibility that the photometric variability in the non-eclipsing DPVs could reflect a beat phenomenon in multiperiodic pulsating stars. This idea

arises from the fact that the long-term periods are also very typical for beat periods of non-radial gravity mode oscillations in B-type stars, the so called slowly pulsating B stars (hereafter SPBs, e.g. Waelkens 1991, De Cat & Aerts 2002). Moreover, De Cat et al. (2000) have shown the case of HD 92287, a single line B-type binary with a circular orbit showing ellipsoidal variations and g-mode pulsations which are easily mixed up in single-band photometry. On the other hand, the position of the target stars in the colour-magnitude diagram (Fig. 11) is very similar to those of a sample of periodically variable B-type supergiants found by Waelkens et al. (1998) from the HIPPARCOS mission. The pulsation hypothesis is particularly relevant now that pulsating B stars have been found in the Magellanic Clouds (Kolaczkowski et al. 2004).

We cannot directly test the presence of very short periods in our sample of DPVs, due to the sampling of the OGLE-MACHO data. In the future we plan to do that, monitoring our targets with higher time resolution. At the moment, the Nyquist frequency is about 0.5 c/d in most cases. However, we can check the presence of periodicities larger than 2 days. For that we have prewithened the light curves shown in Fig. 12 with the binary solution. The binary light curve was obtained by fitting the data with a double sinusoid excluding the main minimum. Residuals to this fit were analyzed searching for multiple periods. No trace of additional periodicities were found apart from the fundamental frequency of the long-term oscillation. For that, and for the following reasons we believe that the pulsation hypothesis based on SPBs or α-Cyg type pulsations is incompatible with the data: (i) The amplitude of the long-term variations is almost constant in most cases, this is not the usual case for stars showing the phenomenon of beating of multiple oscillations. (ii) The amplitude of the long-term variability is rather large (about 0.2 mag) when compared with amplitude of SPBs (about 0.02 mag) or even with amplitudes of α-Cyg type supergiants (< 0.1 mag) and it is hard to image how a beat of low amplitude oscillations could produce the observed large amplitude variability. (iii) There is no color dependence in the short-term variability of DPVs, contrary to the pulsations observed in SPBs. (iv) The long-term oscillations are red, contrary to the SPBs pulsations which are blue (v) The periodogram of SPBs looks completely different to the periodograms of DPVs; they clearly show the presence of multiple periods in the range of 1-3 days, and no presence of a long periodicity over 100 days. On the contrary, periodograms of DPVs shows a strong minimum at the long period (indicating a fundamental frequency) and no evidence for multiple periods in the short-period range, except the short-term periodicity that always appears with much less power than the longer one (vi) Concerning α-Cyg type supergiants, like those found by Waelkens et al. (1998), they show multiple periods, and their light curves are highly irregular in shape, and include the presence of microvariability; they do not show the strictly periodic pattern of DPVs characterized by a single short period.

Although the above points argues against SPBs-type or α-Cyg type pulsations, we cannot exclude the presence of very short pulsations of a new nature in these objects, and defer this question for future photometric studies with higher time resolution.

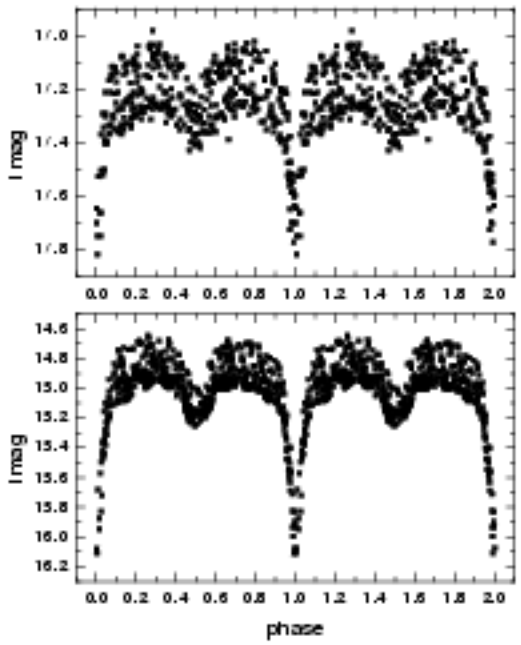

Figure 12. The light curves of OGLE05052263-6852002 (up) and OGLE05200407-6936391 (down) folded with the respective short-term periods. No pre-whitening has been applied in these cases. The vanishing of the long-term variability (noisy pattern) during the main eclipses indicates an origin of this variability in the brighter component.

4.4 On the importance of stellar winds and mass loss rates

It is well known that early B-type giants have significant mass loss rates due to radiatively-driven winds (e.g. Vink et al. 2001). In addition, it has been shown that near-critical rotation could induce extreme mass loss in massive stars even far from the Eddington limit (Aerts et al. 2004). Following these arguments we have explored the possibility that the weakness of the Hβ line could be due to mass loss in some of the DPVs.

In the following, we assume neglectable the contribution of the less luminous star and any other light source to the overall light of the system. Hence the derived parameters refers to the primary, the more luminous star. We calculated the $V \sin i$ from the full line widths of the He I 4471 and Mg II 4481 lines. The results, shown in Table 8, indicate that the stars are rotating with higher velocities than those obtained by assuming corotation with the binary system. The stellar masses derived according to M_{Sel} (Table 4) and using the Maeder & Meynet (1988, 1989) evolutionary tracks are also shown in Table 8, along with the stellar radius, calculated from the $\log g$ values. The mass loss rates given in Table 8 are derived from Vink et al. (2001) assuming $Z_{LMC} = 1.0$ and $Z_{SMC} = 0.1$. The $V \sin i$ values indicates that the stars are rotating at a large fraction of the critical velocity (Table 8, column 5). On the other hand, the stars are far from the Eddington limit (Table 8, column 6). Applying the recipe given by Aerts et al. (2004) for mass-loss rates of rotating

massive stars, we found that the rotational contributions to the total mass loss rates are less than $\log \dot{M} = 0.02$ and therefore neglectable for our objects. However, looking in the $\dot{M}$ values of Table 8 we find that they are comparable to the $\dot{M}$ values observed in Be stars in the equatorial regions, so the presence of a radiatively supported gaseous envelope around the primary is compatible with our result, and could in principle explain the weakness of the Hβ line by filling by emission from an optically thin gas envelope. This envelope should produce an emission line pattern with a steep Balmer decrement, which would be observed as selective filling-up; larger amounts of emission should be observed in lower order Balmer lines, as apparently occurs. The contribution to the continuum by an optically thin envelope could be neglectively small in optical wavelengths. If this view is true, future observations of the Hα line or the IR continuum should reveal unambiguously the emitting envelope.

4.5 A link between long-term variability and Be stars?

In Section 4.2 we excluded the possibility of an accretion disc around the secondary star. However, the possibility of a gaseous envelope around the primary, as mentioned in Section 4.4, and the vanishing of the long-term oscillation during the eclipse of the primary, could indicate an origin in a disc-like envelope around a Be-star primary. In order to check this possibility, we calculated if there is enough room for a disc around the primary star. Using classical formulae for close binary systems (e.g. Warner 1995), we estimated the fraction of the Roche lobe filled by the brighter component. From the values of this fraction, given in Table 8, we conclude that most systems have room for a disc, but a very small disc.

It is hard to relate the long-term variability with the one-armed oscillations observed in Be star discs. They have quasi-period between 2-11 years and occurs in discs extending to several stellar radius (e.g. Okazaki 1997). Also the colour of these oscillations in Be star discs are in general remarkably blue (Mennickent et al. 1997). Is then possible that tidal forces acting on this disc could cause long-term oscillations different in nature to the one-armed oscillations? An origin in a cool disc-like envelope could be consistent with the red colour observed in this variability.

5 CONCLUSIONS

Evidently, we don't have the complete solution for this very interesting phenomenon at this moment. Our findings support the thesis that double periodic variables are close binary systems consisting of B type primaries and secondaries. We identify the shorter periodicity in non-eclipsing systems as the ellipsoidal variation of the brighter component which fills a considerable fraction of their Roche lobe. A better clarification of the phenomenon needs of further observations especially in the infrared in order to reveal the nature of the cooler companion and the possible existence of a disc-like envelope in some of the systems. A cool gaseous envelope could explain the weakness of the absorption lines and the flattening of the continuum. Another problem which remains to be solved refers to the origin of the long-term photometric period in these systems. We have identified the source if this variability in or around the primary star. However, we dont know if they imply a new kind of stellar pulsation or some kind of oscillation in a cool emitting envelope around the primary star. Further spectroscopic studies are necessary to investigate the nature of the long term variation and the peculiar intrinsic color excesses in order to understand how these binary systems evolve and how their evolution depend on mass, mass exchange and chemical content. High time resolution photometry is also desirable, since it could provide insights about the pulsation properties of these stars.

The main conclusions of the analyses reported in the previous sections can be summarized as follows:

- Spectra of 7 double periodic blue variables are consistent with B-type stars of luminosity class between IV and III.
- Radial velocity variations of the Hβ absorption line reveal the binary nature of OGLE05060009-6855025 and OGLE05195898-6917013.
- In these cases the short-term periodicities are consistent with ellipsoidal variations of the brighter component.
- The dynamical solution and the analysis of the short-term light curve of these objects indicate a mass for the cooler companion between 6-10 $M\odot$, excluding the possibility for accretion disc formation. This means early B-type secondaries for these systems.
- A study of the rotational velocities of the brighter components indicate rotational velocities larger than the expected for synchronization with the binary orbit.
- Estimates of the companion temperature based on the light curve analysis indicate that they are lower by factors 0.8-0.9 than those of the hotter components. This finding is compatible with B-type companions and with the absence of significant colour variations during the orbital cycle.
- The large fraction of eclipsing binaries (6 cases) found in the whole sample of 33 double periodic variables suggests that the probability of identifying this kind of variable depends on the system inclination, being larger for high inclination systems.
- We suspect that many of the Type-3 stars (i.e. those showing long-term periodicities) reported by M02 and not classified as double periodic variables are the same kind of system but seen at lower inclination. This is consistent with the interpretation of the short-term photometric modulation as ellipsoidal variations of the brighter component.
- We find the long-term variability practically disappear during the main eclipse in the eclipsing DPVs. This means that the origin of the long-term variability is in or around the primary star.
- No known pulsation mechanism can explain the long-term variations. However, the presence of very short pulsations in the primary star cannot be discarded with the present data.
- The mass-loss rates for DPVs are comparable with those observed in the equatorial regions of Be stars.
- The origin of the apparent filling of the absorption lines and flatness of some continuums could be due to free-free and free-bound emission from a cool circumstellar envelope. Further studies of this new class of variables and its relation with other periodic blue variables are needed to clarify this point.

Table 8. $V \sin i$ based on the width of the HeI 4471 and MgII 4481 lines and the stellar mass, equatorial radius, lower limit for the ratio between the rotational velocity and the critical velocity v/v_c, the ratio Γ between the luminosity and the Eddington luminosity and the mass loss rate $\dot{M}$ by radiation driven winds. The ratio between the primary radius and their Roche lobe volume radius is also given.

star	$V \sin i$ (km/s) or note	M ($M_\odot$)	R ($R_\odot$)	v/v_c	Γ	$\dot{M}$ ($M_\odot$/yr)	R/R_L
OGLE00451755-7323436	noisy	11	6.5	NA	0.04	-10.7	0.5
OGLE00553643-7313019	270	11	4.1	0.46	0.04	-11.7	0.3
OGLE05060009-6856025	240	7	16.4	1.03	0.02	-11.0	1.1
OGLE05155332-6926581	140	5.5	12.1	0.58	0.01	-11.2	0.9
OGLE05195828-6917013	180	5.5	7.2	0.58	0.01	-11.2	0.7
OGLE05313130-7012584	> 300	7	9.8	1.00	0.02	-10.8	0.5
OGLE05410942-7002215	noisy	19	32.2	NA	0.11	-8.7	1.6

ACKNOWLEDGMENTS

We acknowledge useful insights provided by the referee, Conny Aerts, which helped to improve the scientific discussion in this paper, especially concerning the hypothesis of stellar pulsations. RM acknowledges support by Fondecyt grant 1030707. RM, WG. and G.P. acknowledge support from the Chilean FONDAP Center for Astrophysics 15010003. B. Sabogal acknowledges support by Programa MECE Educación Superior UCO0209.

REFERENCES

Aerts C., Lamers H. J. G. L. M., Molenberghs G., 2004, A&A, 418, 639
Al-Naimiy H. M., 1978, Ap&SS, 53, 181
Barbier D., Chalonge D., 1941, AnAp, 4, 30
Chalonge D., Divan L., 1952, AnAp, 15, 201
Cidale L., Zorec J., Tringaniello L., 2001, A&A, 368, 160
Cox A. N., 2000, Allen's Astrophysical Quantities, Springer, AIP Press
De Cat P., Aerts C., 2002, A&A, 393, 965
De Cat P., Aerts C., De Ridder J., Kolenberg K., Meeus G., Decin L., 2000, A&A, 355, 1015
Didelon P., 1982, A&AS, 50, 199
Divan L,, Zorec J. 1982, ESA-SP, 177
Djuraševi G., Rovithis-Livaniou H., Rovithis P., Georgiades N., Erkapi S., Pavlovi R., 2003, A&A, 402, 667
Eggleton P. P., 1983, ApJ, 268, 368
Flower P. J., 1977, A&A, 54, 31
Frank J., King A., Raine D. J., 2002, in Accretion Power in Astrophysics: Third Edition, by Juhan Frank, Andrew King, and Derek J. Raine. Cambridge University Press.
Kolaczkowski, Z., Pigulski, A., Soszynski, I., et al., in: Variable Stars in the Local Group, IAU Colloquium 193, Proceedings of the conference held 6-11 July, 2003 at Christchurch, New Zealand. Edited by Donald W. Kurtz and Karen R. Pollard. ASP Conference Proceedings, Vol. 310. San Francisco: Astronomical Society of the Pacific, 2004., p.225).
Maeder A., Meynet G., 1988, A&AS, 76, 411
Maeder A., Meynet G., 1989, A&A, 210, 155
McClintock J. E., Petro L. D., Remillard R. A., Ricker G. R., 1983, ApJ, 266, L27
Mennickent R. E., Sterken C., Vogt N., 1997, A&A, 326, 1167
Mennickent R. E., Pietrzyński G., Gieren W., Szewczyk O., 2002, A&A, 393, 887
Mennickent R. E., Pietrzyński G., Diaz M., Gieren W., 2003, A&A, 399, L47
Mennickent R. E., Assmann, P., Pietrzyński G., Gieren W., 2004, in proceedings of the workshop "The Light-Time Effect in Astrophysics", C. Sterken (editor), ASP conference Series, in press
Okazaki A. T., 1997, A&A, 318, 548
Paczyński B., 1971, ARA&A, 9, 183
Russell H. N., 1945, ApJ, 102, 1
Slettebak A., 1985, ApJS, 59, 769
Udalski A., Szymanski M., Kubiak M., Pietrzynski G., Wozniak P., Zebrun K., 1998, AcA, 48, 147
Udalski A., Soszynski I., Szymanski M., Kubiak M., Pietrzynski G., Wozniak P., Zebrun K., 1999, AcA, 49, 223
Vink J. S., de Koter A., Lamers H. J. G. L. M., 2001, A&A, 369, 574
von Zeipel H., 1924, MNRAS, 84, 702
Waelkens C., 1991, A&A, 246, 453
Waelkens C., Aerts C., Kestens E., Grenon M., Eyer L., 1998, A&A, 330, 215
Warner B., 1995, Cataclysmic Variable Stars, Cambridge Astrophysical Series 28, Cambridge University Press
Welch D. L., Cote P., Fischer P., Mateo M., Madore B. F., 1991, AJ, 101, 490
Zebrun K., et al., 2001, AcA, 51, 317
Zorec J., 1986, PhD Thesis, Paris: Universite VII
Zorec J., Briot D., 1991, A&A, 245, 150